Shock Acceleration of the Energetic Particle Background in the Solar Wind

David T. Sodaitis

Physics Department, University of New Hampshire
Durham, New Hampshire, USA

sodaitis@cisunix.unh.edu

ABSTRACT

Lee (1983) described the problem of an interplanetary shock that accelerates protons out of the cold thermal background via the mechanism of second order Fermi acceleration. In this acceleration method, the particle bounces between two converging flows (the upstream and downstream turbulence of the shock) and gains energy in the plasma frame at every encounter with the shock. This presents a view of particle acceleration by interplanetary shocks that joins wave excitation with particle acceleration by using the cold thermal population to provide the seed ions for acceleration. In this theory (1) the asymptotic form of the particle spectrum is a power law dictated by the strength of the shock β, (2) the higher energy protons follow an exponential form as they have insufficient opportunity for acceleration, and (3) low-frequency magnetic waves are excited by the 10 to 200 keV protons. More recent observations of shocks coincident with solar energetic particle (SEP) events (Desai et al. 2003) have shown that shock acceleration may act preferentially on the hot energetic background particles that already have sufficient energy to be advantaged in the injection process at the shock, thus utilizing a possible seed population that benefits from pre-acceleration. We examine a typical interplanetary shock that is coincident with a solar energetic particle population using Advanced Composition Explorer data from February 16-18, 1999 to look for evidence supporting the Lee (1983) theory.

1. Introduction to the Solar Wind

The solar wind consists of a stream of ions and a remnant of the solar magnetic field radiating outward from the sun. It is composed largely of protons and electrons, with some alpha particles and trace amounts of heavier ions (Isenberg 1991). As a result of the gas pressure differential between the sun's corona and interplanetary space, which exerts a force greater than the restraining force of gravity, the solar wind is driven outward. For those of us residing on planet Earth, the solar wind is an important topic for study because it is strongly influenced by solar activity, and it transfers that solar influence "to planets, comets, dust particles, and cosmic rays that are immersed in the wind" (Hundhausen 1995). This means that understanding the solar wind is important for gaining a better understanding a broad range of physical phenomena that occur within the solar system, and especially, here on and within the near space surrounding our own planet Earth. The solar wind has a direct impact on the Earth's space weather, which in turn has important implications for critical technologies and infrastructure that our civilization depends on, including but not limited to communications satellites and the terrestrial power grid.

The classic description of the solar wind consists of three components, a fluid model of the sun's corona which in it's equilibrium state creates a supersonic flow of plasma outward into interplanetary space, "frozen-in" magnetic field lines which are tied to the expanding plasma and and pushed out into space by the solar wind, and the interplanetary shock waves that propagate outward from the sun which are the subject of this research.

1.1. Coronal Heating and Expansion

Observations using x-rays have shown that the sun's corona exists in a very dynamic environment at a temperature in the millions of degrees, much hotter than the actual surface of the sun, the photosphere. (See Figure 1.) The origin of the heating of the corona is still a subject open to much debate, though it is widely believed to be caused by a magnetic mechanism. The fact that the corona is highly dynamic and inhomogeneous may be important for heating (Priest 1995). Regardless of the heating source, given these conditions, hydrostatic models would predict a plasma pressure far away from the sun that is much greater than the pressure in interstellar space, leading to the conclusion that hydrostatic equilibrium cannot exist in this system and the corona must continually expand (Isenberg 1991). Though it is beyond the scope of this paper to go into too much detail, a model of the corona based on a spherically symmetric, steady-state system, consisting of a fully ionized proton-electron gas, taking into account equations of state, and equations for conservation of momentum and particles, produces an equation for the square of the Mach number, $M^2 = nmV^2/\gamma P$ as follows:

$$\frac{M^2-1}{M^2}\frac{dM^2}{dr} = \frac{\left(1+\frac{\gamma-1}{2}M^2\right)\left(4E+\frac{3\gamma-5}{\gamma-1}\frac{GM_s}{r}\right)}{r\left(E+\frac{GM_s}{r}\right)} \tag{1-1}$$

where r = the radial distance from the sun relative to the sun's radius, γ = the polytropic index ($\gamma = 1$ indicates isothermal flow), V = the average weighted electron/proton gas volume, n = the number density of protons and electrons, P = the gas pressure, and E = the total energy (a constant). This differential equation cannot be solved analytically, but the character of the solutions to this equation can be represented topologically (Isenberg 1991) as shown in Figure 2. What this model (Parker 1963; Holzer 1979) tells us is that given the physical environment in the corona, the solar wind must accelerate from subsonic to supersonic speeds, and this has since been confirmed by observations.

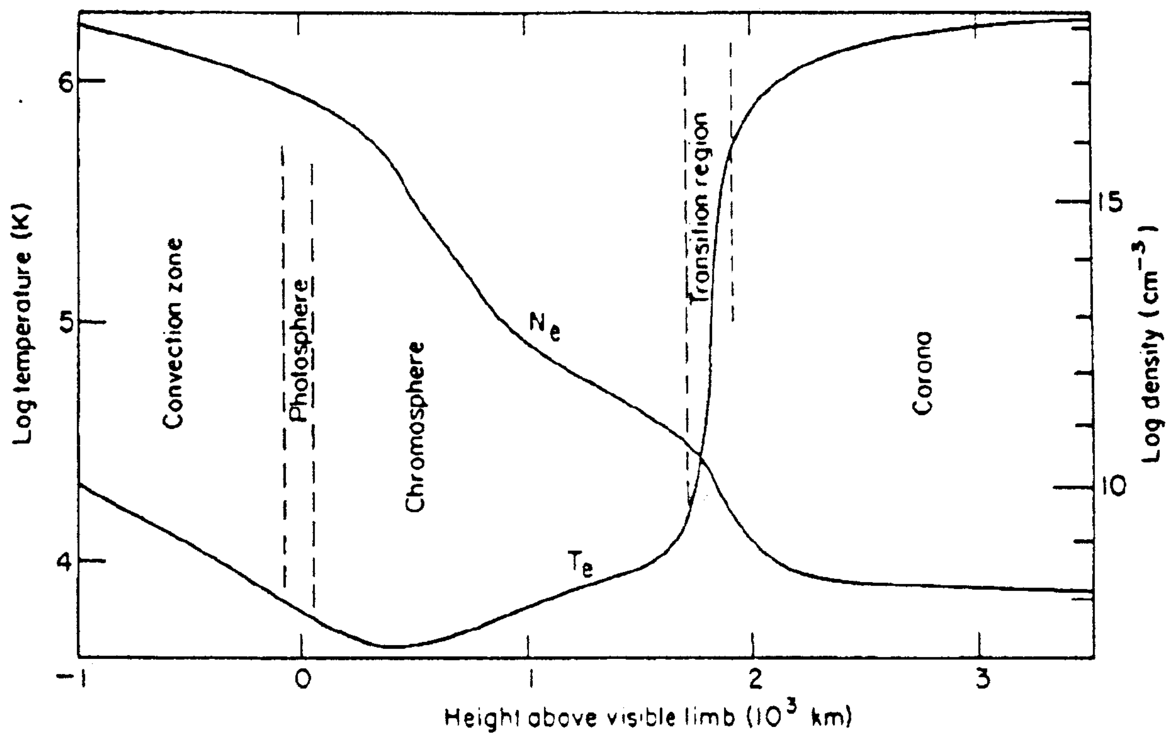

Fig. 1.— Schematic representation of the variation with height of the mean values of temperature and density in the outer layers of the sun (Gabriel and Mason 1982). Note that the temperature of the corona is several orders of magnitude higher than the temperatures of the photosphere and chromosphere.

1.2. The Solar Wind at 1 AU

Embedded in the hot and fast-moving (by terrestrial standards) plasma that is the solar wind is a weak magnetic field emanating from the sun. Due to the angular rotation of the sun (ω), the magnetic field lines carried through interplanetary space become more and more tightly wound as the distance from the sun increases. At 1 AU, $\omega \cdot r \approx 405\,\mathrm{km/s}$, and the average longitudinal and radial components of the magnetic field are almost equal, thus the field lines are oriented nearly parallel to the solar system's ecliptic, but at approximately 45° to a line from the sun to an observer in the ecliptic plane (Hundhausen 1995). As previously mentioned, the sun's coronal heating is not uniform, and depending on local conditions on the sun, as the sun rotates, these variations in coronal activity discharge Solar Energetic Particles (SEPs) at differing speeds, leading to the creation of hot and cold (fast and slow) winds. While the magnetic field compresses with increasing heliocentric distance, the particle density decreases proportionally with R^{-2}. Tables 1 and 2 show some typical characteristics of the solar wind at 1 AU. Especially worth noting is the Alfvén speed, which is the propagation speed of electromagnetic waves with frequencies less than the proton cyclotron frequency, that is, it is the typical speed to which plasma can be accelerated by magnetic forces (Priest 1995). It is important to note because it is embedded in the definition of the subject of this research— interplanetary shocks are defined as transients that propagate through the solar wind at several Alfvén speeds.

1.3. Transients

1.3.1. Interplanetary Shock Waves

From time to time there are major disturbances (time variations) in the solar wind, the most striking of which are interplanetary shock waves that move outward from the sun. Gaining a better understanding of these shock waves is important because as they reach the Earth, they can have

Table 1. Characteristic lengths of the solar wind at 1 AU.(Barnes 1979)

Characteristic length	Typical value at 1 AU	Convection time past spacecraft at 1 AU
Proton Gyroradius	∼ 50 - 100 km	∼ 0.1 s
Electron Gyroradius	∼ 1 - 2 km	$\sim 1\times10^{-2}$ s
Inertial Length	∼ 2 km	$\sim 1\times10^{-2}$ s
Debye Length	∼ 6 m	$\sim 1\times10^{-5}$ s
Proton Mean Free Path	∼ 3 AU	$\sim 1\times10^{6}$ s
Electron Mean Free Path	∼ 0.7 AU	$\sim 1\times10^{5}$ s

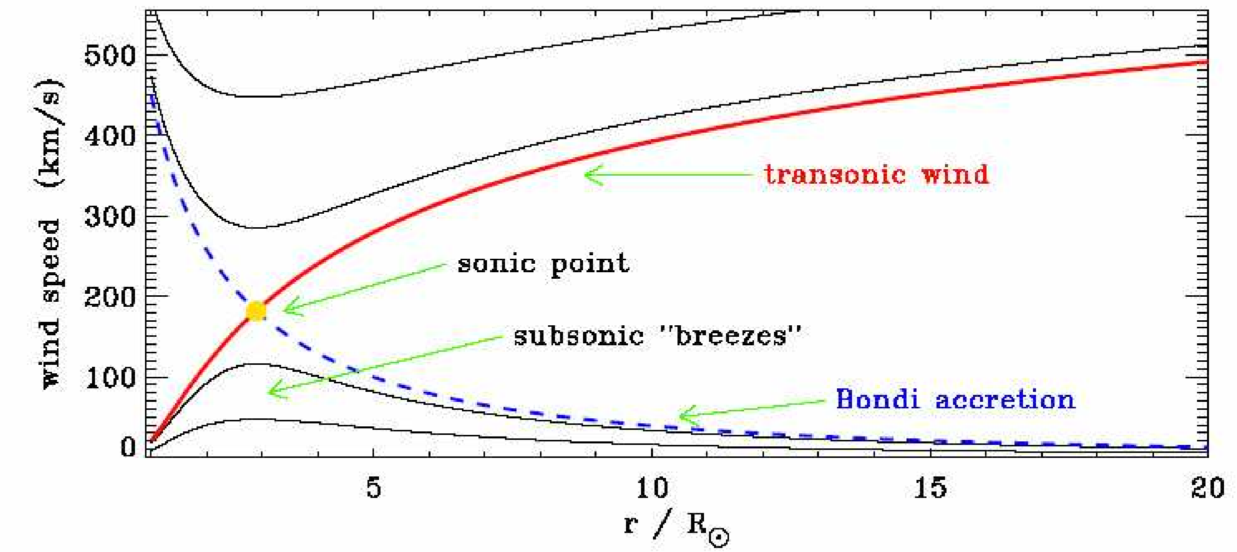

Fig. 2.— Topological analysis of equation 1-1. The only solution that meets the requirement of low speed at the sun and high speed at large radial distances from the sun is the solution passing through the critical “sonic point” labelled “transonic wind” (Isenberg 1991)

.

Table 2. Characteristic speeds of the solar wind at 1 AU. (Barnes 1979)

Characteristic speed		Typical value at 1 AU
Alfvén Speed	$V_A = B/(4\pi m_p n)^{1/2}$	$\sim$ 50 km/s
Ion Sound Speed	$V_S = [(5/3)k(T_e + T_p)/m_p]^{1/2}$	$\sim$50 km/s
Proton Thermal Speed	$V_{thp} = (3kT_p/m_p)^{1/2}$	$\sim$50 km/s
Electron Thermal Speed	$V_{the} = (3kT_e/m_e)^{1/2}$	$\sim$2000 km/s

drastic impacts on the behavior of the Earth's space weather. With the aid of space probes outside the Earth's magnetosphere such as the Advanced Composition Explorer, these shocks are detected by the sudden changes in the solar wind speed, density, temperature, and magnetic-field strength that they bring with them, with abnormal values of these parameters lasting for for a day or more after the initial onset. Due to the dynamic nature of the corona, the energetic particles leaving the corona and entering the solar wind have differing kinetic energies, and thus travel at different speeds, due to the particular local conditions on the Sun which give rise to different methods of particle acceleration. When the bulk of the ions is moving fast enough to overtake a slower moving population, an interplanetary shock is formed. As the shock front overtakes the slower-moving solar wind in front of it, it accelerates and heats the plasma that it sweeps up, thus transferring energy and momentum to a larger and larger piece of the solar wind. In other words, we can say that shocks are "discontinuities" that satisfy basic conservation laws needed to transition from supersonic to subsonic flow. In addition to dissipating their energy through solar wind heating, shocks leave behind an irreversible increase in entropy. Eventually, as such shocks deplete their momentum and energy, they decelerate as they move outward through planetary space (Hundhausen 1995).

1.3.2. Coronal Mass Ejections

One of the proposed mechanisms for the birth of interplanetary shock waves is the phenomenon known as a Coronal Mass Ejection (CME). A Coronal Mass Ejection is a major temporal disturbance in the corona that creates a self-contained plasmoid leaving the sun's corona at high speed. At a distance of 1 AU, CMEs typically move thru solar wind at several times the Alfvén Speed. This creates a shock front at the leading edge of the plasmoid. CMEs have magnetospheric and space weather implications outside range of this thesis, but merit mentioning as the probable origin for interplanetary shocks. Figure 3 shows an example of a CME[1].

1.3.3. The Rankine - Hugoniot Relations

Although the solar wind is a collisionless plasma, in certain ways a magnetized plasma can behave in ways that correspond to an ordinary gas or fluid. This is the realm of magnetohydrodynamics (MHD). While MHD cannot describe the structure of a shock itself, it can describe the downstream state in relation to the upstream state. Originally derived to describe a collisional gas, the Rankine-Hugoniot relations describe the behaviour of shock fronts normal to an oncoming flow. Named after nineteenth century physicists William John Macquorn Rankine and Pierre Henri Hugoniot, the idea is to consider one-dimensional, steady flow of a fluid subject to the Euler equations (similar to the Navier-Stokes equations but with zero viscosity and heat conduction),

[1]Picture thanks to SOHO (ESA and NASA). See `http://sohowww.nascom.nasa.gov/`

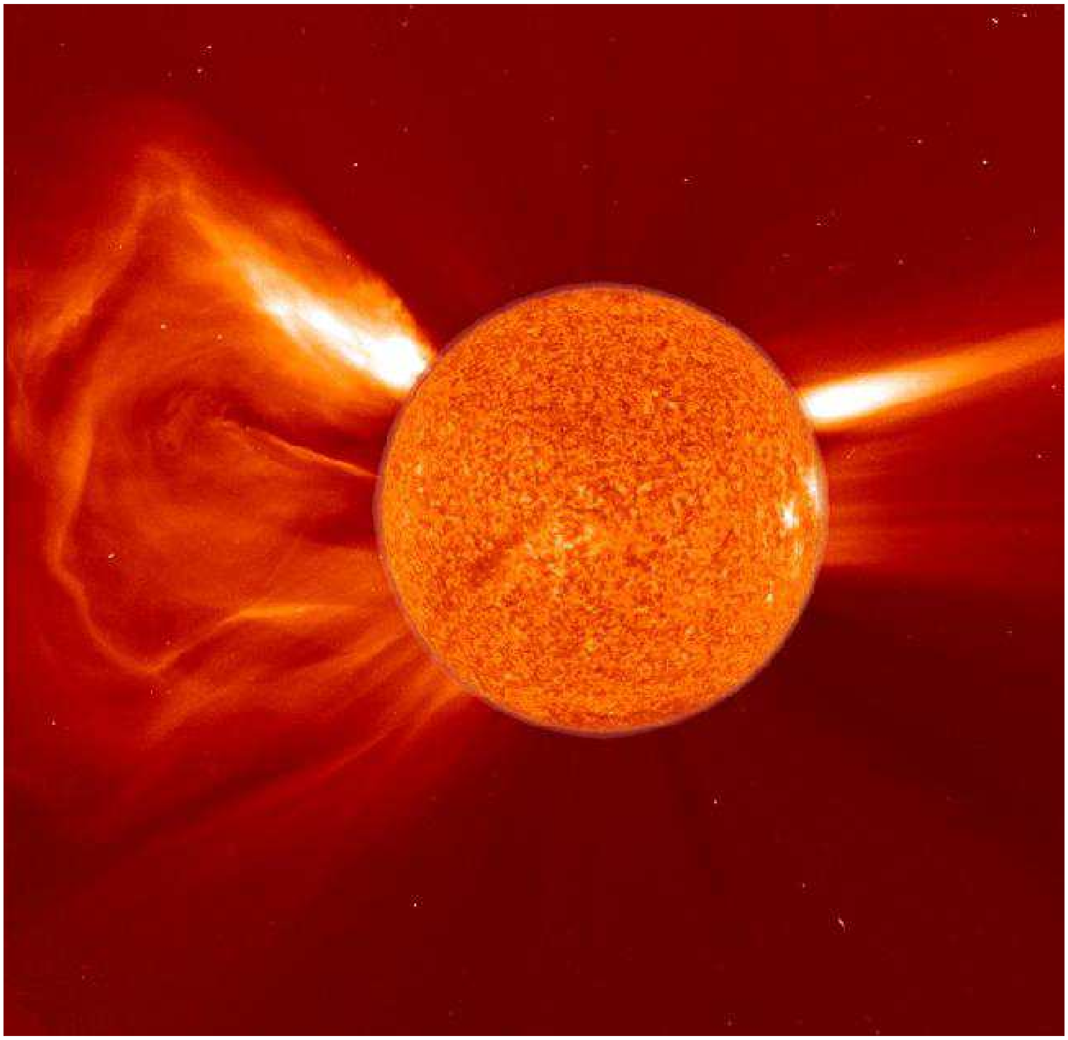

Fig. 3.— A bright and expansive coronal mass ejection (CME) unfurled itself on January 24, 2007. As seen in SOHO's LASCO/C2 (Large Angle and Spectrometric Coronagraph), the bright front emerged in the shape of an arc from behind the occulting disk but soon expanded into a ragged, bulbous shape with lots of structural lines inside it. The source of this CME was an active region that had just began to rotate into view the next day. An Extreme ultraviolet Imaging Telescope (EIT) 304 Angstrom image of the Sun taken at nearly the same time was enlarged and superimposed on the occulting disk. **Courtesy of SOHO/LASCO consortium. SOHO is a project of international cooperation between ESA and NASA.**

and require that mass, momentum, and energy are conserved. In the case of the solar wind, a collisionless plasma, the Rankine-Hugoniot relations cannot uniquely predict the downstream state in terms of the upstream conditions, but they are useful in describing the basic parameters of a shock, and deciding on whether or not there is a shock at all (Burgess 1995). Table 3 shows the Rankine-Hugoniot relations used to compute shock parameters. In the years since these equations were first developed, various mathematical methods for implementing a Rankine-Hugoniot analysis have been developed. For this particular research the Szabo (1994) method of computing the shock characteristics was performed. The Szabo technique uses a nonlinear least squares fitting technique that incorporates observations of plasma conditions such as normal momentum flux, energy density flux conservation, plasma density, velocity, and magnetic field data (Szabo 1994).

The shock characteristics produced by this analysis of the shock of February 18, 1999 are found in Table 4 and also online[2]. The most relevant of these shock characteristics to the subject of this study are the magnetic-field-to-shock-normal angle, $\theta_{Bn} \approx 50^{\circ}$, indicating an oblique shock, and the compression ratio, a comparison of upstream and downstream densities, found to be $r_n \approx 2.9$. In addition, the shock's upstream Mach number M_A is worth noting. For this shock $M_A \approx 3.4$, which means that it is propagating through the solar wind at 3.4 times the Alfvén speed.

2. Shock Acceleration Theory

Interplanetary shocks are propagating disturbances that represent solar wind transitions where the inflowing speed (in the frame of the shock) is supersonic (super-Alfvénic), and the outflowing speed is subsonic (sub-Alfvénic). This process leads to density compression. Additionally, the magnetic field is tied to particle flow, so the magnetic field gets compressed and any pre-existing magnetic fluctuations are also compressed and intensified in the downstream flow.

2.0.4. Particle Propagation through the Solar Wind

In the solar wind, particle propagation is often described in terms of a mean magnetic field and fluctuations in that field. Individual particles follow the mean field to first order and interacts with fluctuations to second order. The phenomenon is inherently nonlinear: Fluctuations lead to scattering, while particle motion can alter fluctuations. This nonlinear aspect also makes resonance possible. The resonance condition is $kv_p + \omega = \pm\Omega_{pc}$ where k is the wave vector and $\Omega_{pc} = eB/mc$. Resonant particle scattering requires (1) resonance and (2) magnetic energy. Because scattering behind the shock is intensified, resonant particle scattering tends to occur far upstream but not far downstream. This situation creates a converging flow with "scattering centers" upstream and

[2]The ACE Science Center, Transients section, located at `http://www.ssg.sr.unh.edu/mag/ace/ACElists/obs_list.html`

Table 3. Rankine - Hugoniot Relations. (Szabo 1994)

Equation of state	Quantity compared across shock
$\Delta[\rho(v_n - V_s)] = 0$	Conserved mass flux
$\Delta[\mathbf{B} \cdot \hat{\mathbf{n}}] = 0$	The normal component of the magnetic field
$\Delta[\rho(v_n - V_s)\mathbf{v_t} - \frac{B_n}{\mu_0}\mathbf{B_t}] = 0$	Tangential component of the momentum flux
$\Delta[P + \ = \rho(v_n - V_s)(\hat{\mathbf{n}} \times \mathbf{B_t})] = 0$	Tangential component of the electric field
$\Delta[P + \frac{B_t^2}{2\mu_0} + \rho(v_n - V_s)^2] = 0$	Normal momentum flux
$\Delta[\rho(v_n - V_s)\left(\frac{\mathbf{V}-V_s\hat{\mathbf{n}}}{2} + \frac{\gamma}{\gamma-1}\frac{P}{\rho} + \frac{B^2}{\mu_0\rho}\right) - \frac{B_n(\mathbf{V}-V_s\hat{\mathbf{n}})\cdot\mathbf{B}}{\mu_0}] = 0$	Energy Flux

Note. — These equations contain upstream and downstream parameters, as the jump across the shock is noted by $\Delta[\,]$. The parameters include plasma mass density (ρ), plasma bulk velocity (v), shock speed along the normal (V_s), shock magnetic field (B), isotropic thermal gas pressure (p), and the ratio of specific heats (γ). Subscripts n and t reference normal and tangential components. See Szabo (1994) for more details.

Table 4. Characteristics of the shock event of February 18, 1999 ~2:00 UT.

Parameter		Computed Value
Shock speed in the spacecraft frame (km/s)	V	671 ± 26
Shock speed in the upstream plasma frame (km/s)	V	278 ± 23
Compression Ratio	r_n	2.9 ± 0.1
Upstream magnetic field to shock normal angle (°)	θ_{Bn}	50 ± 2
Upstream Mach number	M_A	3.4 ± 0.3

Note. — Data from the ACE Science Center website, Transients section.

downstream. Each reflection leads to energy gain by the particles. Much like a ping-pong ball rapidly bouncing between a paddle an a wall as the paddle moves closer to the wall, repeated scattering in the converging flow increases the particle energy.

2.1. Seed Ions

The theoretical basis for the research presented in this paper comes from Lee (1983) and to a lesser extent Desai et al. (2003). The Lee theory assumes acceleration out of the "cold" thermal background and predicts growth of transverse fluctuations with equal right- and left-hand waves while Desai et al. (2003) argues in favor of acceleration of a hot solar energetic particle (SEP) background based on the similarity of the ionic composition of shock accelerated particles with those of SEP populations. (SEPs are high-energy protons, electrons, and ions accelerated away from the sun at energies from tens of keV up to the GeV range.) The next section takes a closer look at the Lee theory:

2.1.1. The Lee Model of Interplanetary Shocks

When describing the properties of large numbers of particles with different velocities, it is convenient to speak in terms of phase space density, that is, how many particles are in a six dimensional volume where $d\mathbf{v}d\mathbf{r} = dv_x dv_y dv_z dx dy dz$. This is also referred to as the single-particle distribution function. The number of particles in the differential volume at phase position $(\mathbf{v}, \mathbf{r})$ is then expressed as $f_s(\mathbf{r}, \mathbf{v}, t)d\mathbf{v}d\mathbf{r}$ and the number of particles of type s per unit ordinary volume (number density) is found by integrating over all possible velocities (Kivelson 1995):

$$n_s(\mathbf{r}, t) = \int f_s(\mathbf{r}, \mathbf{v}, t) d\mathbf{v}.$$

Using this descriptive method of phase space, Lee created a simple but useful model of a planar interplanetary shock as follows:

In the normal incidence frame, that is, considering planar stationary shock acceleration as fixed in the frame of the shock front, let

$$f(v, z > 0) = f_\infty + (f_0 - f_\infty)\, e^{-\zeta} \tag{2-1}$$

where $f_\infty(v)$ is specified as the upstream advected omnidirectional distribution function, and

$$\zeta(z) = \int_0^z \left[V/K_{zz}(z', v)\right] dz' \tag{2-2}$$

represents a dimensionless expression of the normal distance z from the shock. At the shock front itself,

$$f_0 = f(v, z = 0) = \beta \int_0^v f_\infty(v') \left(\frac{v}{v'}\right)^{-\beta} \frac{dv'}{v'} \tag{2-3}$$

where

$$\beta = \frac{3r_n}{r_n - 1} \tag{2-4}$$

and r_n is the shock's compression ratio. Far upstream of the shock, the seed population distribution can be described by a combination of remnant suprathermals and cold thermal seed ions

$$f_\infty(v) = f_{\text{remnant suprathermals}}(v) \quad + \quad \frac{\xi n_{p,\text{ solar wind}}}{4\pi v_{p,0}^2}\delta\left(v - v_{p,0}\right)) \tag{2-5}$$

in order to model injection out of the solar wind and advected suprathermals where ξ is the injection fraction, typically about 10^{-3} to 10^{-2}. Using an upstream distribution function containing a double power law with a velocity breakpoint (v_0), we then have:

$$f_\infty(v) = \begin{cases} Cv^{-\alpha} \quad + \quad \frac{\xi n_p}{4\pi v_p^2}\delta\left(v - v_p\right) \quad , & v < v_0 \\ Cv_0^{-\alpha}\left(\frac{v}{v_0}\right)^{-\gamma} \quad + \quad \frac{\xi n_p}{4\pi v_p^2}\delta\left(v - v_p\right) \quad , & v > v_0 \end{cases} . \tag{2-6}$$

For $v < v_0$, the distribution function at the shock is described as in equation 2-3 by

$$f_0 = \beta \int_{v_\epsilon}^{v} C(v')^{-\alpha}\left(\frac{v}{v'}\right)^{-\beta}\frac{dv'}{v'} \quad + \quad \beta\int_{v_\epsilon}^{v}\frac{\xi n_p}{4\pi v_p^2}\delta\left(v' - v_p\right)\left(\frac{v}{v'}\right)^{-\beta}\frac{dv'}{v'} \tag{2-7}$$

where v_ϵ is a very small velocity close zero representing the speed of the solar wind in the shock frame. Assuming $v_\epsilon < v_p < v$, this yields a phase space distribution at the shock of

$$f_0(v < v_0) = \frac{C\beta}{\beta - \alpha}\left(v^{-\alpha} - v_\epsilon^{\beta-\alpha}v^{-\beta}\right) \quad + \quad \frac{\beta\xi n_p v_p^{\beta-3}}{4\pi}v^{-\beta} \tag{2-8}$$

while for $v > v_0$,

$$f_0 = \beta\int_{v_\epsilon}^{v_0} f_\infty(v')\left(\frac{v}{v'}\right)^{-\beta}\frac{dv'}{v'} \quad + \quad \beta\int_{v_0}^{v} f_\infty(v')\left(\frac{v}{v'}\right)^{-\beta}\frac{dv'}{v'} \tag{2-9}$$

which becomes

$$\begin{aligned} f_0 &= C\beta v^{-\beta}\int_{v_\epsilon}^{v_0}(v')^{-\alpha}\left(v'\right)^{\beta-1}dv' \\ &+ \quad C\beta v^{-\beta}v_0^{\gamma-\alpha}\int_{v_0}^{v}(v')^{-\gamma}\left(v'\right)^{\beta-1}dv' \\ &+ \quad \beta\frac{\xi n_p}{4\pi v_p^2}v^{-\beta}\int_{v_\epsilon}^{v}\delta\left(v' - v_p\right)\left(v'\right)^{\beta-1}dv' \end{aligned} \tag{2-10}$$

and then at the shock front

$$f_0(v > v_0) = \frac{C\beta}{\beta-\alpha}\left(v_0^{\beta-\alpha} - v_\epsilon^{\beta-\alpha}\right)v^{-\beta} \quad + \quad \frac{C\beta}{\beta-\gamma}\left(v_0^{\gamma-\alpha}v^{-\gamma} - v_0^{\beta-\alpha}v^{-\beta}\right) \quad + \quad \frac{\beta\xi n_p v_p^{\beta-3}}{4\pi}v^{-\beta}. \tag{2-11}$$

Now, for $v < v_0$, we have

$$f_0 - f_\infty = \frac{C}{\beta - \alpha}\left(\alpha v^{-\alpha} - \beta v_\epsilon^{\beta-\alpha} v^{-\beta}\right) \quad + \quad \frac{\beta \xi n_p v_p^{\beta-3}}{4\pi} v^{-\beta} \tag{2-12}$$

and for $v > v_0$, we get

$$f_0 - f_\infty = \frac{C\gamma}{\beta - \gamma} v_0^{\gamma-\alpha} v^{-\gamma} \quad + \quad \frac{C\beta\,(\alpha - \gamma)}{(\beta-\alpha)(\beta-\gamma)} v_0^{\beta-\alpha}\, v^{-\beta} \quad - \quad \frac{C\beta}{\beta-\alpha} v_\epsilon^{\beta-\alpha}\, v^{-\beta} \quad + \quad \frac{\beta \xi n_p v_p^{\beta-3}}{4\pi} v^{-\beta}. \tag{2-13}$$

Given these distribution functions in phase space, it is also possible to change from the distribution function $f(v)$ to intensity spectrum $J(E)$ using the conversion relation

$$J(E) = \frac{2E}{m^2}\, f\left(\sqrt{\frac{2E}{m}}\right) \tag{2-14}$$

where

$$v = \sqrt{\frac{2E}{m}} \tag{2-15}$$

which allows us to rewrite the expressions for the two power laws in terms of energy. Below the energy breakpoint, using the relation $E_0 = \frac{1}{2} m v_0^2$, the intensity spectrum then becomes

$$J_0(E) - J_\infty(E) = \frac{C\alpha}{m(\beta-\alpha)}\left(\frac{2E}{m}\right)^{1-\alpha/2} \quad + \quad \left[\frac{\beta \xi n_p v_p^{\beta-3}}{4\pi m} - \frac{C\beta v_\epsilon^{\beta-\alpha}}{m(\beta-\alpha)}\right]\left(\frac{2E}{m}\right)^{1-\beta/2} \tag{2-16}$$

while above the breakpoint, it is

$$J_0(E) - J_\infty(E) = \left[\frac{C\beta(\alpha-\gamma)}{m(\beta-\alpha)(\beta-\gamma)} v_0^{\beta-\alpha} + \frac{\beta \xi n_p v_p^{\beta-3}}{4\pi m} - \frac{C\beta}{m(\beta-\alpha)} v_\epsilon^{\beta-\alpha}\right]\left(\frac{2E}{m}\right)^{1-\beta/2} + \frac{C\gamma}{m(\beta-\gamma)} v_0^{\gamma-\alpha}\left(\frac{2E}{m}\right)^{1-\gamma/2} . \tag{2-17}$$

At the shock itself, the intensity spectrum for $E < E_0$ is given by

$$J_0(E) = \left[\frac{\beta \xi n_p v_p^{\beta-3}}{4\pi m} - \frac{C\beta}{m(\beta-\alpha)} v_\epsilon^{\beta-\alpha}\right]\left(\frac{2E}{m}\right)^{1-\beta/2} \quad + \quad \frac{C\beta}{m(\beta-\alpha)}\left(\frac{2E}{m}\right)^{1-\alpha/2} \tag{2-18}$$

while for $E > E_0$,

$$J_0(E) = \left[\frac{C\beta}{m(\beta-\alpha)} v_0^{\beta-\alpha} - v_\epsilon^{\beta-\alpha} + \frac{\beta\xi n_p v_p^{\beta-3}}{4\pi m} - \frac{C\beta}{m(\beta-\gamma)} v_0^{\beta-\alpha} \right] \left(\frac{2E}{m}\right)^{1-\beta/2} + \frac{C\beta}{m(\beta-\gamma)} v_0 \left(\frac{2E}{m}\right)^{1-\gamma/2} \quad . \tag{2-19}$$

Using Equations 2-16, 2-17, 2-18, and 2-19 along with Equations 2-1 and 2-14, it is then possible to describe the evolution of the intensity spectra with increasing spatial distance upstream of the shock, as implied by $\zeta(z)$. However, it may be more illustrative to note the behavior of the spectra just at the shock front itself. For $E < E_0$, the Lee theory implies[3] that the intensity spectrum will behave as

$$J_0(E) \sim E^{1-\alpha/2} + E^{1-\beta/2} \tag{2-20}$$

while for $E > E_0$:

$$J_0(E) \sim [\alpha - \gamma] E^{1-\beta/2} + E^{-\gamma/2}. \tag{2-21}$$

What equations 2-18, 2-19, 2-20, and 2-21 tell us is that the intensity spectra seen at the shock front are determined by the shock parameter β, which itself is determined by the shock compression ratio, as well as conditions far upstream in the undisturbed solar wind, that is, the exponents α and γ, which describe the upstream advected omnidirectional distribution function (a double power law) for suprathermals. The Lee model describes the accelerations of a composite population of hot SEP ions and cold thermal ions using a power law spectrum, assuming a seed ion distribution composed of a hot power law background (remnant suprathermals) with a cold thermal core (Equation 2-5). Acceleration of the seed population produces the phase space distribution in Equations 2-8 and 2-11. This means that when cold thermal seed ions are accelerated and produce a more intense spectrum than the hot seed ions, the final spectrum will largely be determined by the shock compression parameter β. However, when the hot SEP seed ions produce a more intense spectrum than the cold seed ions, the resultant spectrum is a lifted background spectrum that maintains the spectral index (assuming the suprathermal power law index γ is smaller than the shock compression parameter β).

3. Data Analysis

For this research, we examined Advanced Compositiion Explorer (ACE) spacecraft measurements in the vicinity of interplantary shocks, and selected for study a shock that is coincident with a long-lived solar energetic particle (SEP) event. (For a detailed description of on the ACE mission,

[3]It is convenient to drop the cold thermal terms (produced by integrating the delta functions), since they refer to very low energies (below 1 keV).

see Stone et al. (1998).) Our data analysis is divided into three components: (1) an analysis of the shock properties computed with an improved Rankine-Hugoniot method (Szabo 1994) (2) an analysis of the magnetic waves using ACE MAG data, and (3) an analysis of the energetic particles using ACE EPAM/SWEPAM measurements.

3.1. Shock Properties

The shock analysis has already been described above in Section 1.3.3. In future efforts, using the Szabo (1994) method to compute the shock parameters will play a much larger role, but presently we are content to note that the shock we will study is an oblique shock (see Table 4) that can realistically be expected to show a prolonged (that is, lasting approximately one hour or more) foreshock.

3.2. Magnetic Field Wave Analysis

Using data from the ACE Magnetic Fields Experiment (MAG), we use the same techniques of magnetic wave analysis as performed by Smith et al. (2006a,b) and Hamilton et al. (2008) that were originally developed for studies of interplanetary turbulence. That is, we coordinate the analysis of magnetic field fluctuations with the approaching interplanetary shock. We perform a pre-whitened Blackman-Tukey analysis based on the Fourier transform of the two-point autocorrelation function with a post-darkening correction factor in mean field coordinates (Belcher and Davis 1971; Bieber et al. 1996). Using the resulting magnetic spectra, we are able to (1) fit a power law index to the trace spectrum, and (2) compute the variance anisotropy. We also compute the polarization spectrum in the form of magnetic helicity. See Figure 9 for an example of the many magnetic power spectra produced.

3.3. Energetic Particles

Our analysis of energetic particle data uses Electron Proton Alpha Monitor (EPAM) measurements from the ACE spacecraft with 5 minute resolution. Although we use both the LEMS30 (the sunward looking sensor) and the LEMS120 (the anti-sunward looking sensor) data, here we present only the LEMS30 results, since the LEMS120 analysis is virtually identical. We focus on the P1 through P5 EPAM channels with the energy resolution listed in Figure 5 and Table 5, and compute the average intensity and intensity spectrum for the EPAM data. The average intensity for each channel from P1 through P5 is the average taken over the eight directional sectors. (There are 8 sectors for each channel where a sector is a look direction of width $360°/8$.) The intensity spectrum is then obtained by fitting a double power law as a function of particle energy to the intensity of the P1 through P5 measurements. Since visual inspection of the intensity spectra shows two distinct power laws, we do this in two subsets: P1 through P3 and P3 through P5.

3.4. Data Analysis Summary

In summary, the above analyses yield the following insights:

1. We can compute the change in magnetic power with distance from the shock.
2. We can compute the changing magnetic fluctuation anisotropy.
3. We can look for changes in the polarization spectrum associated with the growth of wave energy.
4. We can compute the energetic particle intensity.
5. We can fit the particle intensity spectra to obtain functional forms.
6. We can compare all of the above with the predictions of theory above.

3.5. Results

The motivation for this research was to look for evidence supporting the Lee (1983) theory of cold seed ion acceleration or the hot seed ion acceleration theory of (Desai et al. 2003), both of which seek to explain the source of seed ion populations for interplanetary shocks. To accomplish this, we examined a typical interplanetary shock from 1999 coincident with a Solar Energetic Particle (SEP) population using data recorded by the Advanced Composition Explorer (ACE) satellite, which detects protons over a range of energies. The shock chosen for study occurred on day 49 of 1999. Based on a Rankine-Hugoniot analysis, it is an oblique shock with $\theta_{Bn} \sim 50^\circ$ and compression ratio $r_N \sim 2.9$ (see Table 4). These parameters imply an intensity spectrum $J(E) \sim E^{-1.25}$ for cold seed ion acceleration.

Figure 5 gives an overview of the EPAM and MAG data. The top two panels in Figure 5 show ACE EPAM data recorded over several days during a shock event, first displayed in a linear scale and then in a logarithmic scale, while the third plot from the top shows the anisotropy in the EPAM data. The first panel makes evident the onset of an energetic solar particle (ESP) event and the duration of the shock, while the solar energetic particle (SEP) onset is made evident in the 2nd panel. Note that the anisotropies for all five EPAM channels converge towards zero as the shock approaches. The shock event that is the subject of this paper occurs at Day 49.08333. The second panel from the top shows that there was also an earlier (albeit much smaller) shock event at 48.2639. This shock has not yet been successfully analyzed, but it is far enough upstream that it probably does not play an important role. The bottom two panels in Figure 5 were computed from ACE MAG data, and show the magnetic power (integrated as in the spectra in Figure 9) and the variance anisotropy in the MAG data. These plots show that there is a rise in magnetic power before the shock, and that the variance anisotropy is high in the elevated power interval, observations which are both consistent with the Lee theory.

Figure 6 provides a wider context for understanding the results using data from Days 47 through 49, while Figure 7 shows the data from Day 49 in a similar manner to Figure 6, but in greater detail. In this series of plots, the shocks are marked with dashed vertical lines. Figure 6 shows both shocks, the earlier shock at 48.2639, and the second (main) shock at 49.0833. Noteworthy at both shocks is the rise in intensity ($J(E)$), rise in magnetic field magnitude (B), and slight rotations in the magnetic field direction (δ is the north/south angle and λ is the latitude of the B measurement). This figure also shows a rise in the fluctuation level at the shocks, as represented by B_{rms} which contains the root-mean-squared fluctuations computed every $16\,s$ using $3\,v/s$ data, as well as a rise in solar wind speed (V_P), rise in density (N_P), and rise in temperature (T_P) as is to be expected given the classical description of shocks. In this figure, as well as in Figure 7, β_P is the ratio of magnetic to kinetic energy, V_A is the Alfvén speed, and M_A is the Alfvén Mach number of the flow, which tends to hide the shock effect. All are classic indicators of a shock, and the rise in V_A (along with a decline in M_A) behind the second shock at 49.0833 is typical of the Interplanetary Coronal Mass Ejections (ICMEs) that drive interplanetary shocks, while the high fluctuation level in the ICME (B_{rms}) is atypical. Previously, in Table 4, the upstream Mach number of the shock which is the subject of this study was noted. For clarification, it is worth pointing out that the M_A plots in Figures 6 and 6 do not show this Mach number. These plots show the Mach number of the flow in the spacecraft frame, not the solar wind frame. These M_A plots show that the flow upstream of the second shock is slowly decreasing, which presents a relatively simple situation that eliminates other flow-associates sources of magnetic waves, making this particular shock attractive for analysis. However, the constant variation in the magnetic field direction (δ , λ) is a potential source of complication to predicting the energetic ion foreshock.

Showing a subsection of the data contained in Figure 5, Figure 8 is a more detailed plot displaying the EPAM intensity data recorded closest to the shock. This plot shows that the ion foreshock seems to extend just about 2 hours upstream of the shock (notice how the intensity spectrum flattens) and is fairly constant, though concurrently there are some north/south variations the magnetic field during this time, indicated in Figure 6. Making a closer comparison of this interval of data with the same interval in the B_rms plot of Figure 6, one also can see that the magnetic fluctuations rise along with intensity, which is a general prediction of Lee, and indicates that the shock is propagating through a locally clean and fairly constant situation.

Figure 9 shows just two of many magnetic spectra compiled in a database of this and other shock events for this research. In each plot, starting from the top down, is shown the the trace of the power spectrum, two perpendicular components, the parallel component, and the magnitude of the magnetic field spectrum along with power law fits to two different frequency intervals, plotted as straight lines slightly above each spectral plot. Below each spectra is a plot of the polarization signature. In both spectral plots, the slight flattening of high frequency tails is indicative of a noise spectrum (Hamilton et al. 2008), which becomes more pronounced during the shock event. When comparing the undisturbed spectra to the spectra at the shock, the change in spectral amplitude of the parallel component and the the flattening of the slope of the magnitude spectra are also very pronounced.

Figures 10 through 13 represent snapshots in time of this same EPAM data plotted as intensity spectra, with double power law fits. Table 6 displays the power law fits from Figures 10 through 13, which show how the low-energy power law index steepens dramatically during a shock, while the higher energy power law changes very little in slope, but tends to rise and fall in amplitude. This supports the (Lee 1983) theory, but indicates that the Desai theory may be at work at higher energies. At the shock itself (Figure 12, Day 49.08333), the power law index of the low energy spectrum is in reasonable agreement with the prediction based on β, which expects $J_0(E) \sim E^{-1.25}$.

Table 5. Energy Resolution of the Electron Proton Alpha Monitor (EPAM) Instrument

Channel	Energy range of particles detected	Color code used in Figures
P1	47 to 65 keV	Blue
P2	65 to 112 keV	Green
P3	112 to 187 keV	Red
P4	187 to 310 keV	Cyan
P5	310 to 580 keV	Magenta

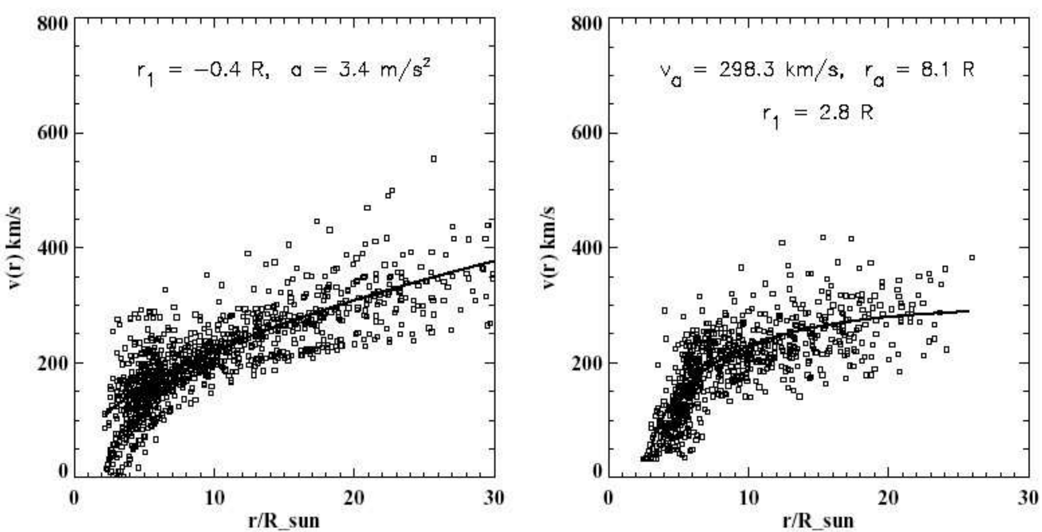

Fig. 4.— Acceleration of the solar wind caused by coronal heating. The acceleration is more rapid closer to the corona and then diminishes (Sheeley et al. 1997).

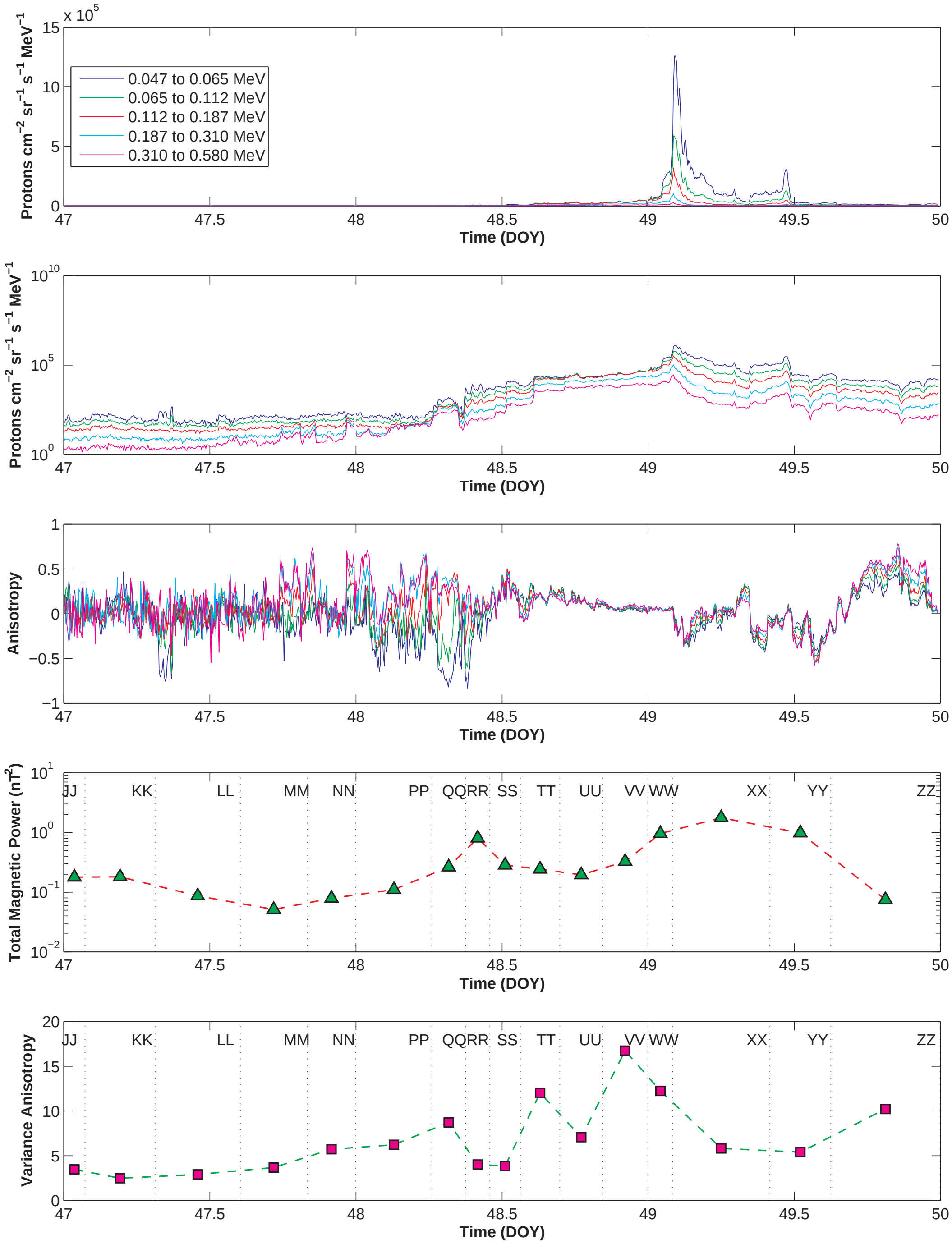

Fig. 5.— The top two plots show time series EPAM data from the ACE satellite for days 47, 48, and 49 in 1999. The shock event occurs about two hours into day 49. The third plot down shows the anisotropy. The lower two plots show magnetic power and anisotropy calculated over the noted intervals (see Figure 9 for spectra corresponding to the JJ and WW intervals).

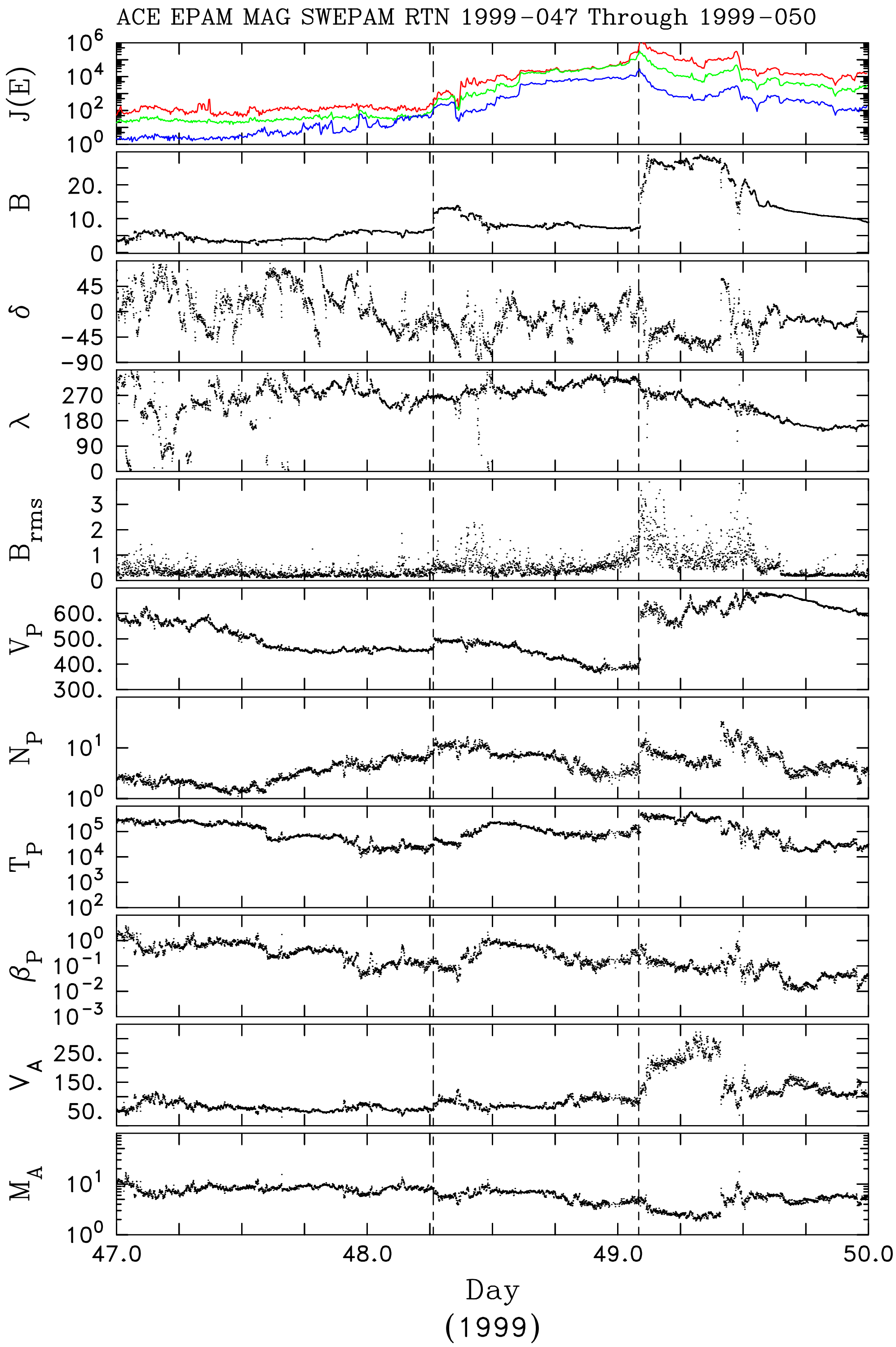

Fig. 6.— EPAM, SWEPAM, and MAG data recorded by the ACE satellite over a three day period starting on February 16, 1999.

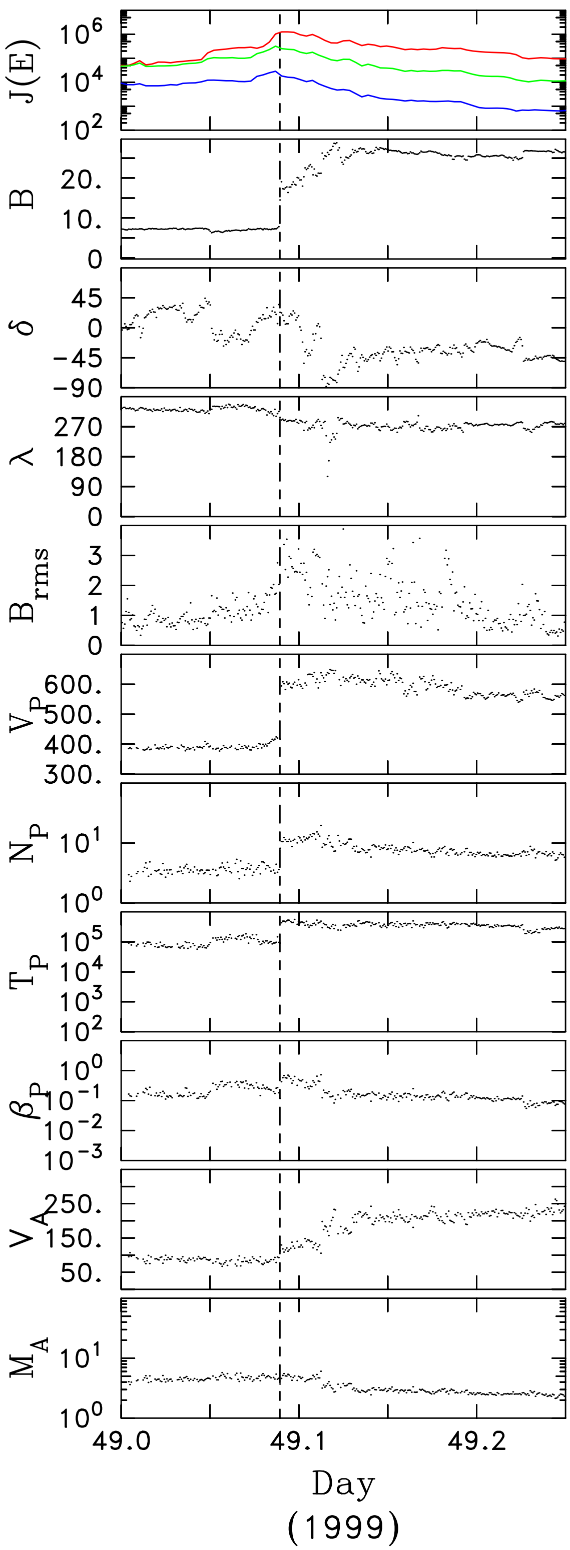

Fig. 7.— A closer look at the data recorded on February 18, 1999.

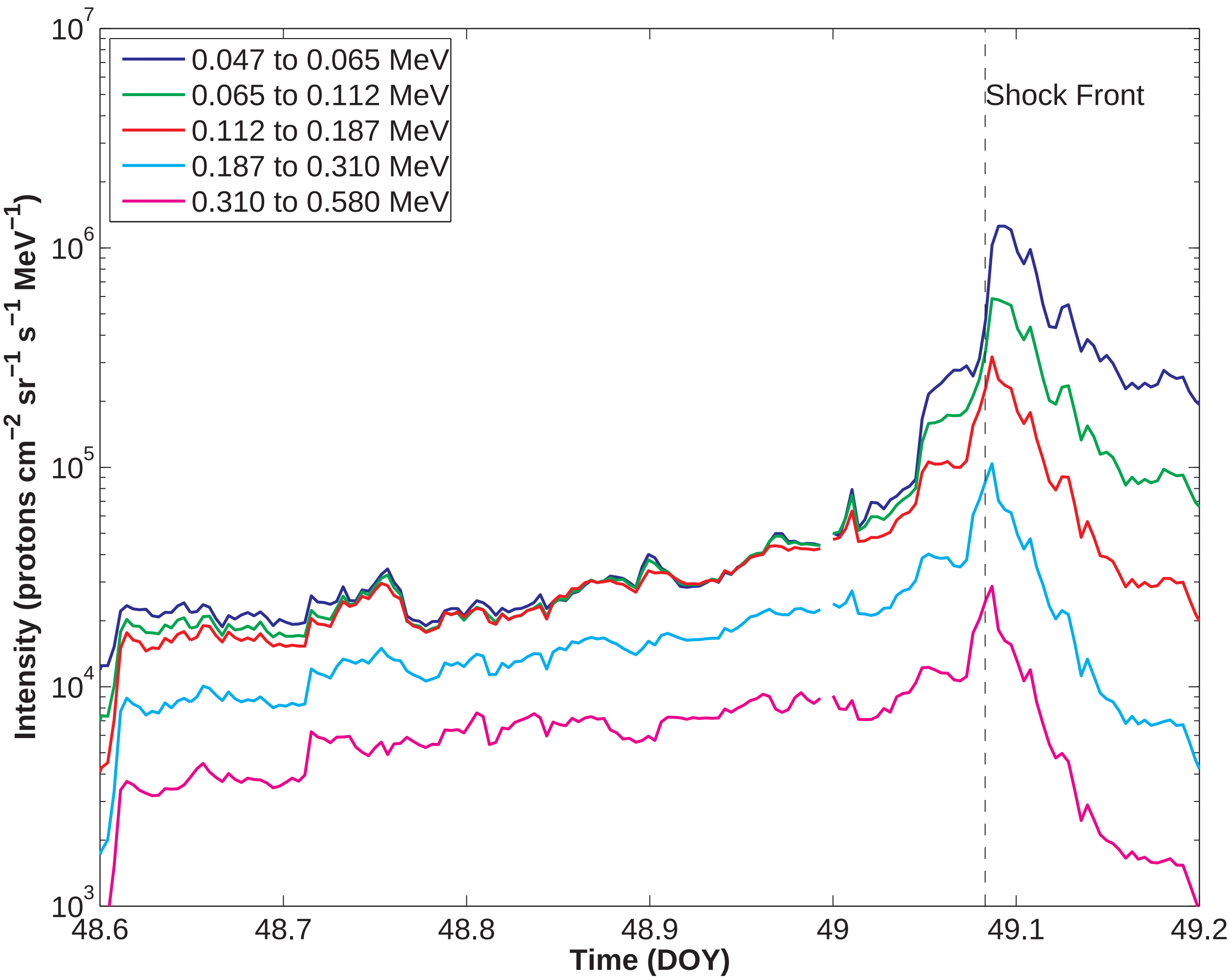

Fig. 8.— A detailed plot of ACE's EPAM data recorded during the shock event of February 18, 1999. The shock front at 49.08333 is indicated with a dashed line. This data is also plotted as intensity spectra in Figures 10 through 13.

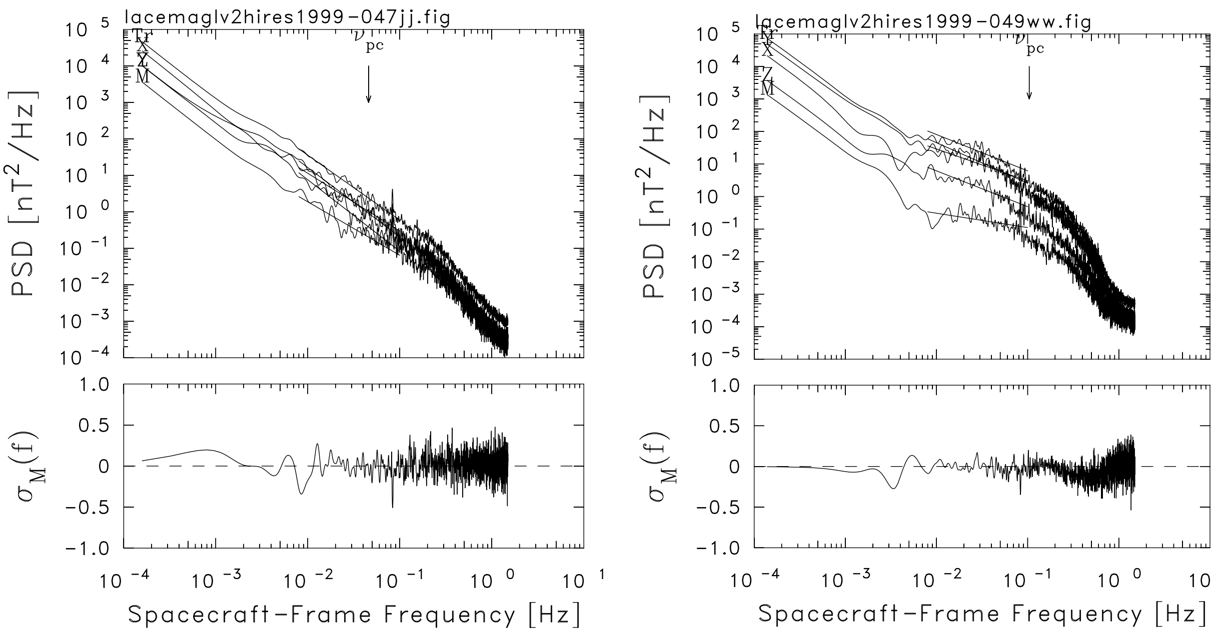

Fig. 9.— Magnetic power spectra computed over the given intervals. In each plot, starting from the top down, is shown the the trace of the power spectrum, two perpendicular components, the parallel component, and the magnitude of the magnetic field spectrum along with power law fits, plotted as straight lines slightly above each spectral plot. Also shown below each spectrum is the normalized magnetic helicity, $\sigma_M(f)$, or polarization signature. The left spectrum is typical of an undisturbed solar wind, that is, two power law regions broken at the onset of dissipation. The right spectrum shows enhancement due to wave energy with an odd polarization signature, which is worth noting in that it differs from the prediction of Lee. The arrow labelled ν_{pc} indicates the proton cyclotron frequency, or the frequency at about which one expects to see waves due to streaming ions coming off the shock, and is approximately where the spectrum deviates from a power law. The change in variance anisotropy is also evident by comparing the two spectra, as a shift in the relation between parallel and perpendicular components is visible.

Table 6 displays the power law indices from Figures 10 through 13, and shows how the power law index for lower energies increases in steepness (becomes more negative) much more rapidly than the index for higher energies. Figure 14 displays this same behavior graphically and in much greater detail, using dual power law fits for every 5 minute interval of EPAM data, and plotting the indices vs. time. Dashed lines show how the the rate of increase for lower energies (channels P1 P2 P3) is much greater than those for higher energies (channels P3 P4 P5), in agreement with the Lee theory.

4. Conclusions

The Lee (1983) theory of shock acceleration predicts that thermal particle acceleration will reach a distribution dependent on the shock compression ratio. However, if the background energetic ions are more intense than what the cold ion source can achieve, then re-acceleration of these particles will preserve the background power law. We find evidence for both processes.

An analysis of this particular shock event on February 18, 1999 strongly suggests that in this event a cold ion seed population dominates the accelerated population close to the shock front. As predicted by the Lee (1983) theory, protons with Energy $<$ 250 keV show evolving index and intensity spectra leading to a power law index determined by the shock compression ratio. On the other hand, protons with Energy $>$ 250 keV show little evidence of an evolving spectral index, but do show increasing intensity as shock approaches, consistent with hot background ion acceleration. This is only one of approximately 40 shocks studied so far, but this albeit limited study suggests that future investigation of additional shock events would also prove fruitful.

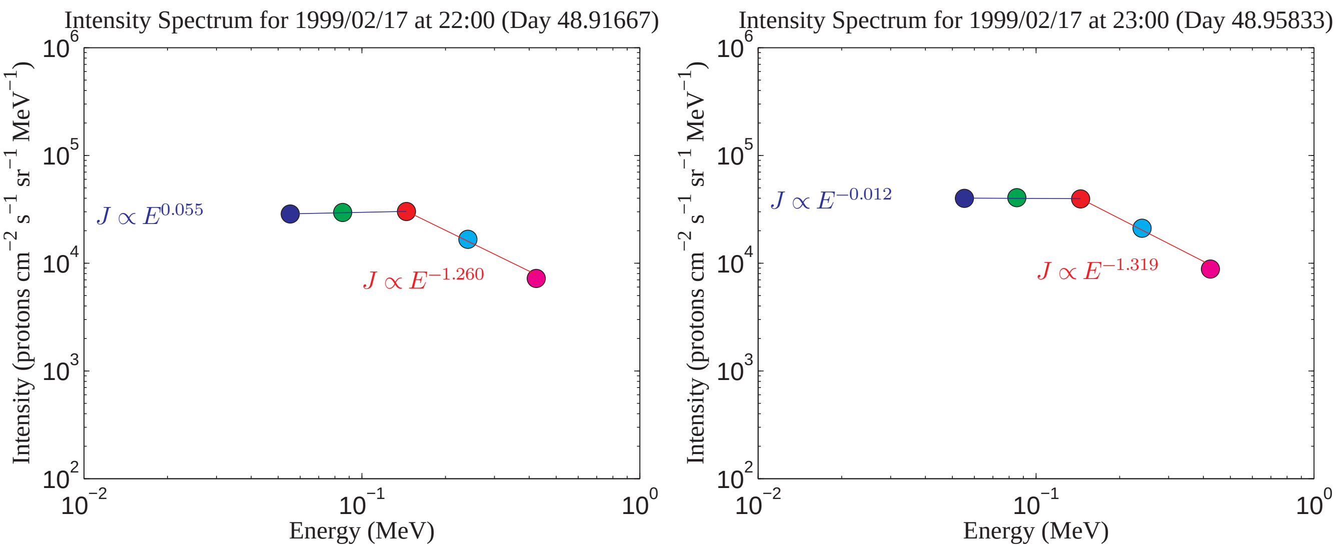

Fig. 10.— Intensity Spectra at day 48.91667 and day 48.95833

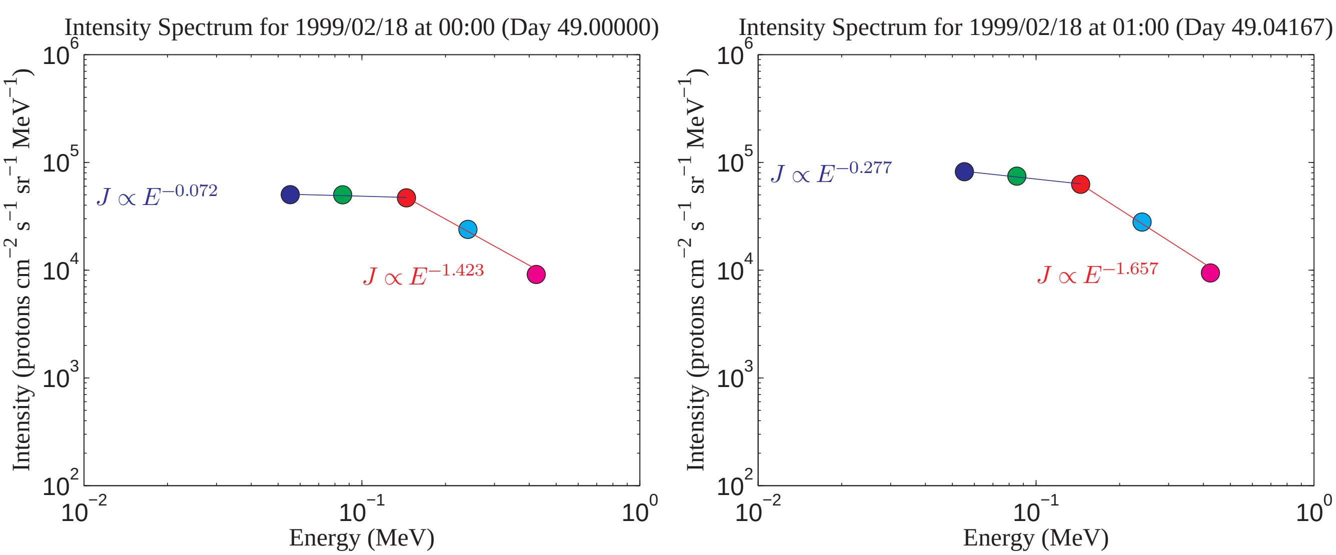

Fig. 11.— Intensity Spectra at day 49.00000 and day 49.04167

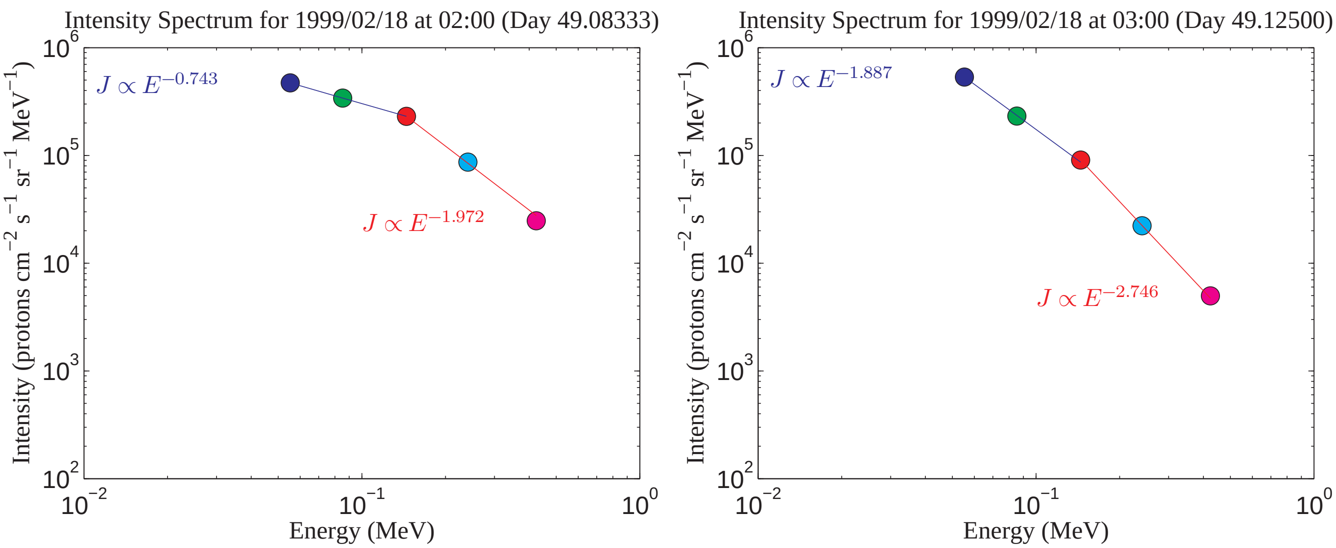

Fig. 12.— Intensity Spectra at day 49.08333 and day 49.125

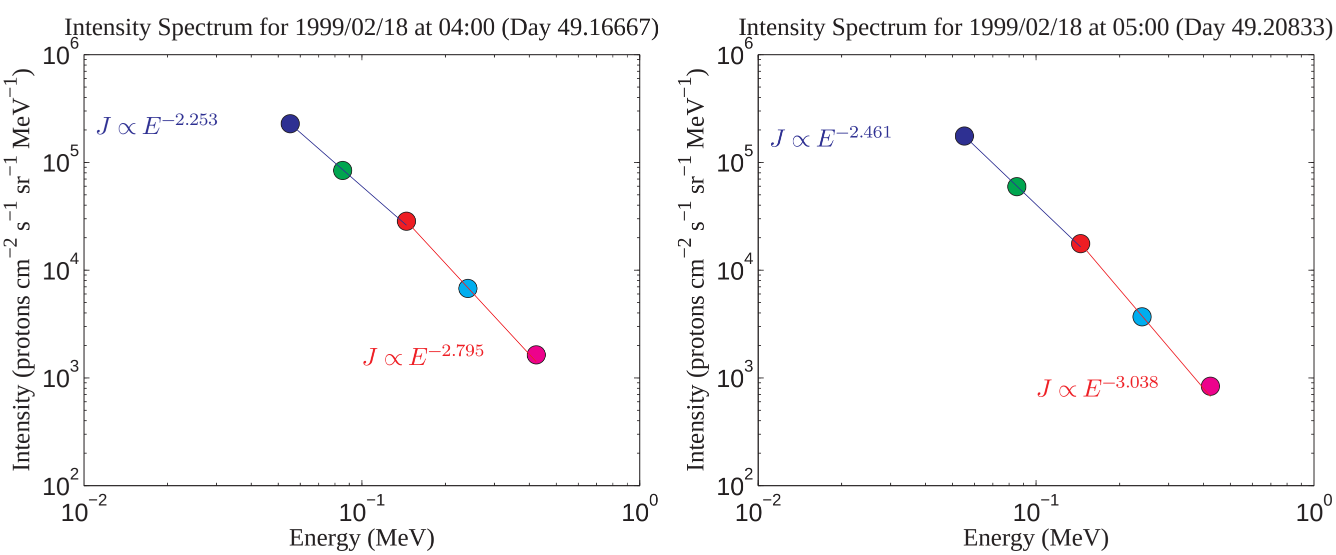

Fig. 13.— Intensity Spectra at day 49.16667 and day 49.20833

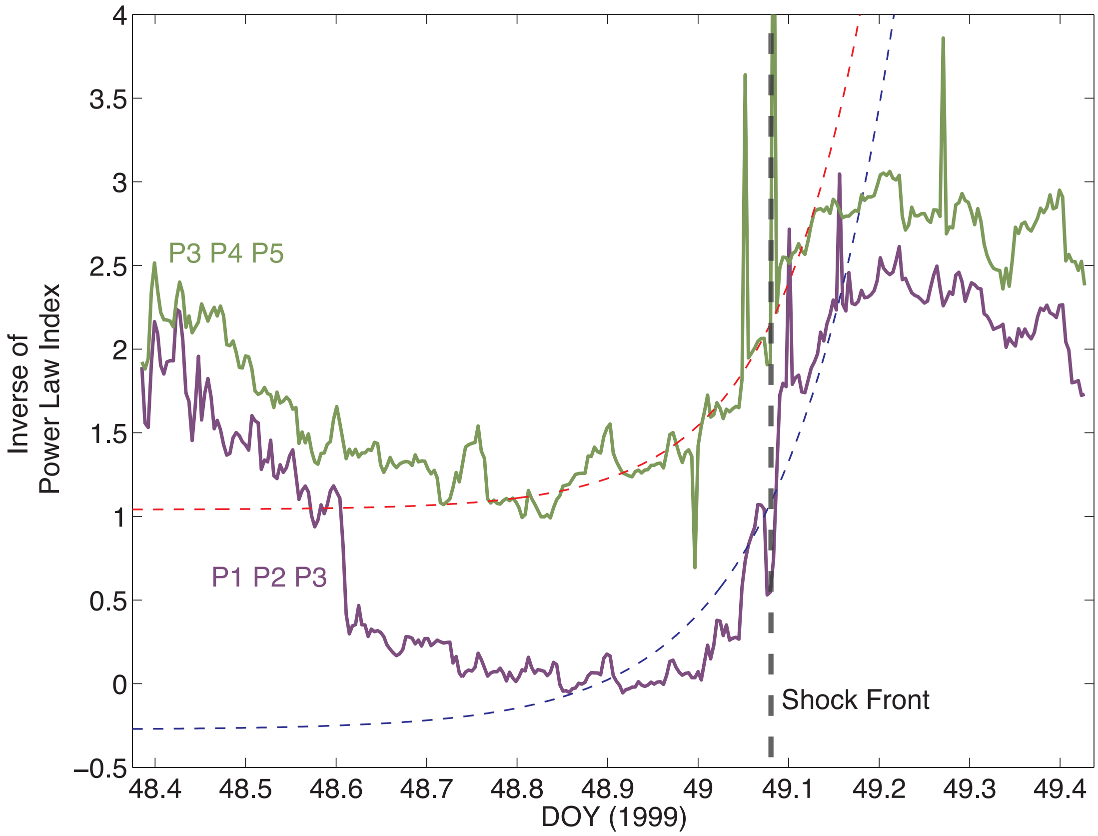

Fig. 14.— Dual power law fits as in Figures 10 through 13 and Table 6 were calculated for every 5 minute interval of EPAM data, and the inverse of the indices from these power law fits were plotted vs. time. Dashed lines show how the the rate of increase (that is, becoming increasingly negative) for lower energies (channels P1 P2 P3) is much greater than those for higher energies (channels P3 P4 P5).

Table 6. Intensity Spectra Double Power Law Fits to $J(E) \propto E^{-\alpha}$

Decimal Day	Start (UT)	End (UT)	Value of α for $E < E_0$	Value of α for $E > E_0$
48.91667	22:00	22:05	-0.055	1.260
48.95833	23:00	23:05	0.012	1.319
49.00000	00:00	00:05	0.072	1.4223
49.04167	01:00	01:05	0.277	1.657
49.08333	02:00	02:05	0.743	1.972
49.125	03:00	03:05	1.887	2.746
49.1667	04:00	04:05	2.253	2.785
49.2083	05:00	05:05	2.461	3.038

Note. — The rows correspond to the sequence of plots in figures 10 through 13. The shock occurs at approximately 02:00 (UT) on Day 49. The last two columns show how just before and after the shock the power law fit for the lower energies increases much more drastically than the power law fit for the higher energies.

The author thanks Professors Charles W. Smith and Martin A. Lee of the University of New Hampshire Space Science Center for their time spent advising him in the writing of this undergraduate thesis.

REFERENCES

Barnes, A., Hydromagnetic Waves and Turbulence in the Solar Wind; *Solar System Plasma Physics*, Vol.1, (Amsterdam: North-Holland Publishing), 1979.

Belcher, J. W., and L. Davis, Jr., Large-amplitude Alfvén waves in the interplanetary medium, 2, *J. Geophys. Res.*, *76*, 3534–3563, 1971.

Bieber, J. W., W. Wanner, and W. H. Matthaeus, Dominant two-dimensional solar wind turbulence with implications for cosmic ray transport, *J. Geophys. Res.*, *101*, 2511–2522, 1996.

Burgess, D., Collisionless Shocks. In *Introduction to Space Physics*, (Cambridge: Cambridge University Press), 1995.

Desai, M. I., G. M. Mason, J. R. Dwyer, J. E. Mazur, R. E. Gold, S. M. Krimigis, R. M. Skoug, and C. W. Smith, Evidence for a Suprathermal Seed Population of Heavy Ions Accelerated by Interplanetary Shocks Near 1 AU, *Astrophysical Journal*, *588*, 1149–1162, 2003.

Desai, M. I., G. M. Mason, M. E. Weidenbeck, C. M. S. Cohen, J. E. Mazur, J. R. Dwyer, R. E. Gold, S. M. Krimigis, Q. Hu, C. W. Smith, R. M. Skoug, Spectral Properties of Heavy Ions Associated with the Passage of Interplanetary Shocks at 1 AU, *Astrophysical Journal*, *611*, 1156–1174, 2004.

Hamilton, K., C. W. Smith, B. J. Vasquez, and R. J. Leamon, Anisotropies and Helicities in the Solar Wind Inertial and Dissipation Ranges at 1 AU, *Journal of Geophysical Research*, *113*, A01106, doi:10.1029/2007JA012559 (2008).

Holzer, T. E., The Solar Wind and Related Astrophysical Phenomena, In *Solar System Plasma Physics*, Vol. 1, (Amsterdam: North-Holland Publishing), 1979.

Hundhausen, A. J., The Solar Wind. In *Introduction to Space Physics*, (Cambridge: Cambridge University Press), 1995.

Isenberg, P. A., The Solar Wind. In *Geomagnetism*, Vol. 4, ISBN 0-12-378674-6, Academic Press, Ltd., 1-85, 1991.

Kennel, C. F., et al., Plasma and energetic particle structure upstream of a quasi-parallel interplanetary shock, *J. Geophys. Res.*, *89*, 5419–5435, 1984.

Kennel, C. F., et al., Structure of the November 12, 1978, quasi-parallel interplanetary shock, *J. Geophys. Res.*, *89*, 5436–5452, 1984.

Kennel, C. F., et al., A test of Lee's quasi-linear theoryof ion acceleration by interplanetary traveling shocks, *J. Geophys. Res.*, *91*, 11,917–11,928, 1986.

Kivelson, M. G., Physics of Space Plasmas. In *Introduction to Space Physics*, (Cambridge: Cambridge University Press), 1995.

Lee, M. A., Coupled hydromagnetic wave excitation and ion acceleration upstream of the earth's bow shock, *J. Geophys. Res.*, *87*, 5063–5080, 1982.

Lee, M. A., Coupled hydromagnetic wave excitation and ion acceleration upstream of interplanetary travelling shocks, *J. Geophys. Res.*, *88*, 6109–6119, 1983.

Lee, M. A., Particle acceleration and MHD wave excitation upstream of interplanetary shocks, *Adv. Space Res.*, *4*, 295–304, 1984.

McComas, D. J., S. J. Bame, P. Barker, W. C. Feldman, J. L. Phillips, P. Riley, and J. W. Griffee, Solar wind electron proton alpha monitor (SWEPAM) for the Advanced Composition Explorer, *Space Sci. Rev.*, 86(1-4), 563, 1998.

Parker, E. N., *Interplanetary Dynamical Processes*, Interscience, New York, 1963.

Priest, E. R., The Sun and its Magnetohydrodynamics. In *Introduction to Space Physics*, (Cambridge: Cambridge University Press), 1995.

Sheeley, N. R. et al., Measurements of Flow Speeds in the Corona between 2 and 30 $R_{\odot}$, *ApJ*, *484*, 472–478, 1997.

Smith, C. W., M. H. Acuña, L. F. Burlaga, J. L'Heureux, N. F. Ness, and J. Scheifele, The ACE magnetic field experiment, *Space Sci. Rev.*, 86(1-4), 613, 1998.

Smith, C. W., K. Hamilton, B. J. Vasquez, and R. J. Leamon, Dependence of the dissipation range spectrum of interplanetary magnetic fluctuations upon the rate of energy cascade, *Astrophys. J. Lett.*, *645*, L85-L88, 2006.

Smith, C. W., B. J. Vasquez, and K. Hamilton, Interplanetary magnetic fluctuation anisotropy in the inertial range, *J. Geophys. Res.*, *111*, A09111, doi:10.1029/2006JA011651, 2006.

Stone, E. C., A. M. Frandsen, R. A.Mewaldt, E. R. Christian, D. Margolies, J. F. Ormes, and F. Snow, The Advanced Composition Explorer, *Space Sci. Rev.*, 86(1-22), 1998.

Szabo, A., An improved solution to the "Rankine-Hugoniot" problem, *J. Geophys. Res.*, *99*, 14,737–14, 746, 1994.
